Distributed State Estimation of Hybrid AC/HVDC Grids by Network Decomposition

Vaibhav Donde, *Member, IEEE*, Xiaoming Feng, *Senior Member, IEEE*, Inger Segerqvist, and Magnus Callavik, *Member, IEEE*

***Abstract*— State estimation for bulk power systems is traditionally formulated and executed as one integrated problem in a control center EMS. This simultaneous approach may present challenges when the concerned network consists of different types of systems operated by different entities (ISO, TSO or utility). A leading example is provided by hybrid AC/HVDC grids. We propose a distributed solution method where the system network is decomposed into several subsystems on which state estimation problems are executed separately and iteratively coordinated through updated boundary information. Hybrid AC/HVDC grids naturally decompose into AC and HVDC subsystems. The proposed method uses a LaGrangian relaxation based approach and block wise Gauss-Seidel solution technique to arrive at a solution. The paper describes the method in the context of HVDC grids based on Voltage Source Converter (VSC) technology. It presents a unified modeling framework for monopole/bipole converter configurations, parallel converters, converter-less DC buses, and wind farm connections. Illustrations and test cases are drawn using hybrid AC/HVDC grids formed by IEEE 39 and 300 bus AC grid networks along with monopole and bipole VSC HVDC grids.**

***Index Terms*—HVDC grids, Energy Management System (EMS), State Estimation (SE), Voltage Source Converter (VSC), LaGrangian relaxation, Gauss-Seidel method, Point of Common Coupling (PCC).**

I. Introduction

Hybrid AC/HVDC grids are composed of AC transmission grids interconnected with HVDC transmission grids. While AC grid represents the traditional power system network, HVDC grid is a state-of-the-art technology that enables transport of bulk power efficiently with greater controllability [1]. Various visions for hybrid grids are laid out and projects are in progress worldwide [2].

In order to monitor and operate a hybrid AC/HVDC grid, state estimation application would be required. Traditionally, power system state estimation is formulated as one integrated problem that is solved at the system control center EMS. However for the newer operating paradigms such as AC/HVDC grids, a decentralized approach could be more pragmatic. It could be of interest to have different parts of the system running their own SE algorithm while exchanging data with other parts of the system. Although the AC grid SE could be modified directly to incorporate the DC grid networks in the model, however this approach would require a major overhaul of the AC grid SE model and software. Leveraging upon a natural decomposition of these hybrid system networks into AC grids and HVDC grids, a less intrusive solution is provided by using a decomposition approach where the AC grid SE undergoes minimal algorithmic modifications and DC grid SE is developed separately, that interacts iteratively with the AC grid SE to arrive at the final state estimate for the hybrid AC/HVDC grid network under consideration. Hereby DC Grids or multiple HVDC links can be integrated into the overall system SE in a flexible way as they are introduced over time by various suppliers. This paper develops a distributed SE algorithm based on network decomposition. Hybrid AC/HVDC grids are considered as a primary example, however the method is applicable to other examples, for instance, an AC grid that is decomposed into several subsystems.

The topic of decomposed SE has been addressed by various researchers in the past. In [1], SE is performed using distributed processing, without using a master coordinator. In [4], LaGrangian multiplier is used to enforce the boundary condition. In [5], a two level (two stage) linear estimation method is proposed. AC/HVDC grid SE is described in [6] using simultaneous approach, with a decoupling in the iterations step in [7]. Technique that allows AC grid SE and HVDC grid SE to be executed separately, but interactively, is missing in these references and that is the focus of this paper. Our approach is based on LaGrangian relaxation and Gauss-Seidel techniques and provides a more straightforward way for implementation while maintaining the same solution as simultaneous approach. Patent application [8] addresses AC/HVDC SE problem by considering the PCC bus states only as part of AC grid, while this paper duplicates PCC bus in AC as well as HVDC grids.

The paper is organized as follows. Section II. and III. introduce hybrid grids at a high level and components of the proposed algorithm, respectively. Section IV. and V. respectively describe the problem formulation and solution approach. Section VII. discusses the HVDC grid modeling followed by Section VIII. that illustrates the method with examples and test cases.

II. Hybrid AC/HVDC Grids

A hybrid AC/HVDC grid is composed of AC grids and HVDC grids interconnected with each other at PCC buses. An example is shown in Figure 1 which depicts two

V. Donde (vdonde@gmail.com) is with PG&E (work performed while at ABB.) X. Feng (xiaoming.feng@us.abb.com) is with ABB USCRC, Raleigh NC 27606 USA. I. Segerqvist (inger.segerqvist@se.abb.com) and M. Callavik (magnus.callavik@se.abb.com) are with ABB PSGS, Västerås, SE-72178, Sweden.

interconnected AC grids (AC1 and AC2) and DC grids (DC1 and DC2). AC grids consist of all the components of a traditional AC transmission grid, namely, synchronous generators, AC transmission lines and transformers, loads and induction motors etc. HVDC grids consist of converter stations, HVDC cables and wind farms. Thus the overall hybrid grid network is decomposed into:

1. *AC grid:* it contains the AC networks up to and including the PCC buses. It may include multiple AC networks, which are not connected to each other through other AC networks, for instance, islanded AC networks, or AC grids that are electrically connected to each other only through DC grids.
2. *DC grid:* it contains the HVDC transmission system and converter stations up to and including the PCC buses. This may include multiple DC networks, which are not connected to each other through other DC networks. For the purpose of this work, HVDC grids operated by Voltage Source Converters (VSC) are considered. A DC grid can lie within an AC grid (e.g., DC1) or interconnect multiple AC grids (e.g., DC2).

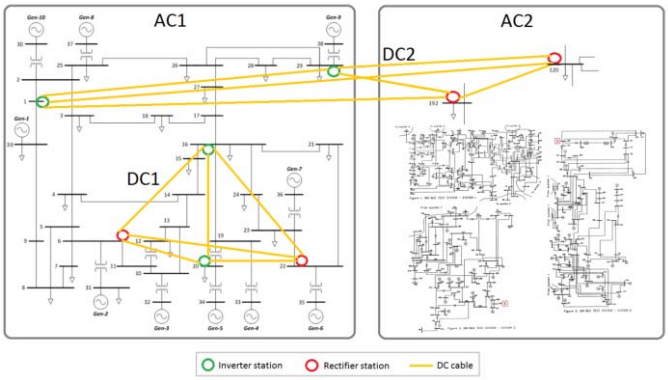

Figure 1: Hybrid AC/HVDC grid example showing two interconnected AC grids and DC grids

III. Components of the Proposed SE Algorithm

A state estimation algorithm is proposed for a hybrid AC/HVDC grid utilizing a natural decomposition of the grid into AC and DC grids. Although the following discussion focusses on hybrid AC/HVDC grids, it is also applicable to other types of hybrid grid networks. The algorithm includes separate AC grid SE and DC grid SE which are executed iteratively by a coordinator program. Specifically, it contains three modules:

1. *AC Grid SE:* this module performs SE on the AC grid based on AC grid model, measurements and certain data obtained from the DC grid as will be discussed later.
2. *DC Grid SE:* this module performs SE on the HVDC grid based on DC grid model, measurements and certain data obtained from the AC grid. It also ensures continuity in the PCC bus states estimated by AC grid SE and DC grid SE.
3. *Coordinator Program:* This program coordinates the data exchange between AC grid SE and DC grid SE. It determines when the iterations between SE grid SE and DC grid SE must be terminated to obtain the final state estimates.

A mathematical derivation of equations underlying the proposed algorithm is described in detail in the next section.

IV. Network Decomposition based Distributed State Estimation Formulation

Consider a power system network that is decomposed into two parts as shown in Figure 2. Without loss of generality, in the present context, the left part represents an AC grid system while the right part represents a DC grid system. After the network decomposition, buses on the boundary, namely the PCC buses, are duplicated and appear in the AC grid as well as in the DC grid. AC grid and DC grid can have multiple subgrids within them.

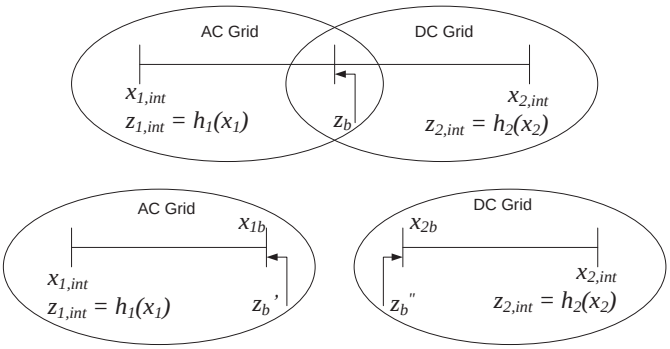

Figure 2: Before and after network decomposition

Table 1 describes the adopted terminology. For the purpose of the analysis that follows, it is helpful to establish the following relationships between the states internal to AC grid and DC grid, and their complete state vectors: $x_1 = \begin{bmatrix} x_{1,int} \\ x_{1b} \end{bmatrix} \Rightarrow x_{1b} = \underbrace{[0 \quad I]}_{K_1} x_1$ and $x_2 = \begin{bmatrix} x_{2,int} \\ x_{2b} \end{bmatrix} \Rightarrow x_{2b} = \underbrace{[0 \quad I]}_{K_2} x_2$. Also, $\frac{\partial h_1(x_1)}{\partial x_{2b}} = 0, \frac{\partial h_2(x_2)}{\partial x_{1b}} = 0.$

Table 1: Variable notations

$x_{1,int}$	States internal to AC grid
x_1	Complete state vector of AC grid (including PCC bus states)
$z_{1,int}$	Measurements internal to AC grid. They are related to the complete state vector of AC grid as $z_{1,int} = h_1(x_1)$
x_{1b}	PCC bus states estimated by AC grid
$z_b{}'$	PCC bus injection measurements as seen from AC grid
$x_{2,int}$	States internal to DC grid
x_2	Complete state vector of DC grid (including PCC bus states)
$z_{2,int}$	Measurements internal to DC grid. They are related to the complete state vector of DC grid as $z_{2,int} = h_2(x_2)$
x_{2b}	PCC bus states estimated by DC grid
$z_b{}''$	PCC bus injection measurements as seen from DC grid

For the state estimation of such hybrid AC grid and DC grid network, Weighted Least Squares (WLS) optimization problem can be written as

$$\min_{x_1,x_2} \left\{ \begin{matrix} 1/2\left(z_{1,int} - h_1(x_1)\right)^T W_1 \left(z_{1,int} - h_1(x_1)\right) \\ +1/2\left(z_{2,int} - h_2(x_2)\right)^T W_2 \left(z_{2,int} - h_2(x_2)\right) \\ +1/2(z_b - h_b(x_1,x_2))^T W_b (z_b - h_b(x_1,x_2)) \end{matrix} \right\} \quad (1)$$

subject to $(x_{1b} - x_{2b}) = 0$

First two terms in the objective function account for measurements internal to AC grid and DC grid respectively, while the third term accounts for the PCC bus injection measurements. The equality constraint maintains continuity at the boundary of the two systems by enforcing the PCC bus states to be identical. According to the terminology adopted, this equality constraint is equivalent to $(K_1 x_1 - K_2 x_2) = 0$.

V. Solution Method

A. LaGrangian Relaxation and Block-wise Gauss-Seidel Method Based Combined AC/HVDC State Estimation

The equality constrained optimization problem in (1) is solved using LaGrangian relaxation in (2). The resulting algorithm as described in this section is realized as the Coordinator Program as referred to in Section III. LaGrange multiplier vector λ has the same dimension as the vector of PCC bus states.

$$\min_{x_1, x_2, \lambda} \begin{Bmatrix} 1/2\big(z_{1,int} - h_1(x_1)\big)^T W_1 \big(z_{1,int} - h_1(x_1)\big) \\ +1/2\big(z_{2,int} - h_2(x_2)\big)^T W_2 \big(z_{2,int} - h_2(x_2)\big) \\ +1/2(z_b - h_b(x_1, x_2))^T W_b (z_b - h_b(x_1, x_2)) \\ +\lambda^T (K_1 x_1 - K_2 x_2) \end{Bmatrix} \quad (2)$$

The PCC bus injection measurement function $h_b(x_1, x_2)$ can be rearranged as $h_b(x_1, x_2) = h_b'(x_1) + h_b''(x_2)$. Let us define $H_b'(x_1) = \frac{\partial h_b'(x_1)}{\partial x_1}$, $H_b''(x_2) = \frac{\partial h_b''(x_2)}{\partial x_2}$.

The first order optimality conditions are given by

$$-H_1(x_1)^T W_1 \Big(z_{1,int} - h_1(x_1)\Big) + K_1{}^T \lambda - H_b'(x_1)^T W_b (\underbrace{z_b - h_b''(x_2)}_{z_b'} - h_b'(x_1)) = 0 \quad (3)$$

$$-H_2(x_2)^T W_2 \big(z_{2,int} - h_2(x_2)\big) - K_2{}^T \lambda - H_b''(x_2)^T W_b (\underbrace{z_b - h_b'(x_1)}_{z_b''} - h_b''(x_2)) = 0 \quad (4)$$

$$(K_1 x_1 - K_2 x_2) = 0 \quad (5)$$

Since $x_1 \in \mathbb{R}^m, x_2 \in \mathbb{R}^n, x_{1b} \in \mathbb{R}^k, x_{2b} \in \mathbb{R}^k$; we have m equations in (3), n equations in (4) and k equations in (5). This *square* system of nonlinear equations can be solved to obtain the system-wide state estimates.

We follow Gauss-Seidel method to solve equations (3)-(5) in order to decouple the solution process for AC grid and DC grid. Specifically, we consider equation (3) separately from equations (4)-(5). This results in the following algorithm.

1. Initialize x_1, x_2 and λ
2. Solve the nonlinear equation (3) using Gauss-Newton algorithm to obtain x_1 at current values of x_2 and . This can be done by running an *inner iteration* loop until convergence or can be terminated after a few or just a single iteration. The inner iteration is based on step update Δx_1 which can be obtained by solving (6).

$$\underbrace{[H_1{}^T \quad H_b{}'^T] \begin{bmatrix} W_1 & \\ & W_b \end{bmatrix} \begin{bmatrix} H_1 \\ H_b{}' \end{bmatrix}}_{\substack{Original\ Gain\ Matrix\ of\ AC\ grid\ SE \\ with\ PCC\ bus\ injection\ pseudo-measurements}} \Delta x_1 = \underbrace{[H_1{}^T \quad H_b{}'^T] \begin{bmatrix} W_1 & \\ & W_b \end{bmatrix} \begin{bmatrix} z_{1,int} - h_1(x_1) \\ z_b' - h_b'(x_1) \end{bmatrix}}_{\substack{Original\ RHS\ of\ the\ AC\ grid \\ with\ PCC\ bus\ injection\ pseudo-measurements}} - \begin{bmatrix} 0 \\ \lambda \end{bmatrix} \quad (6)$$

3. Solve the system of nonlinear equations (4)-(5) simultaneously using Gauss-Newton algorithm to obtain x_2 at current values of λ and x_1. Again, this can be done by running an *inner iteration* loop until convergence or can be terminated after a few or just a single iteration. The inner iteration is based on step updates Δx_2 and $\Delta\lambda$ which can be obtained by solving (7).

$$\begin{bmatrix} \underbrace{[H_2{}^T \quad H_b{}''^T] \begin{bmatrix} W_2 & \\ & W_b \end{bmatrix} \begin{bmatrix} H_2 \\ H_b{}'' \end{bmatrix}}_{\substack{Original\ Gain\ matrix\ of\ DC\ grid\ SE \\ with\ PCC\ bus\ injection\ pseudo-measurements}} & \begin{bmatrix} 0 \\ -I \end{bmatrix} \\ [0 \quad -I] & 0 \end{bmatrix} \begin{bmatrix} \Delta x_2 \\ \Delta\lambda \end{bmatrix} = \begin{bmatrix} \underbrace{[H_2{}^T \quad H_b{}''^T] \begin{bmatrix} W_2 & \\ & W_b \end{bmatrix} \begin{bmatrix} z_{2,int} - h_2(x_2) \\ z_b'' - h_b''(x_2) \end{bmatrix}}_{\substack{Original\ RHS\ of\ the\ DC\ grid \\ with\ PCC\ bus\ injection\ pseudo-measurements}} + \begin{bmatrix} 0 \\ \lambda \end{bmatrix} \\ (x_{2b} - x_{1b}) \end{bmatrix} \quad (7)$$

4. Check convergence
5. If convergence is not achieved, return to step 2. These iterations are terms as *major iterations*.

B. Data Exchange across AC/DC Grid Boundaries

Referring to (6), LaGrange multiplier λ and PCC bus injection pseudo-measurements must be provided to AC grid to estimate x_1. Similarly referring to (7), PCC bus states and injection pseudo-measurements must be provided to DC grid to estimate x_2 and λ. These required quantities must be provided to a grid in question by the other grid from the previous iteration. This results in the following data exchange requirement across the PCC bus boundary:

- *From DC grid to AC grid:* PCC bus LaGrange multiplier λ and injection pseudo-measurements.
- *From AC grid to DC grid:* The PCC bus states and injection pseudo-measurements.

Pictorially, the entire iterative process can be summarized by Figure 3. Note that only the PCC bus state, PCC bus measurements and PCC bus LaGrange multipliers need to be exchanged, resulting in a minimal data exchange requirement.

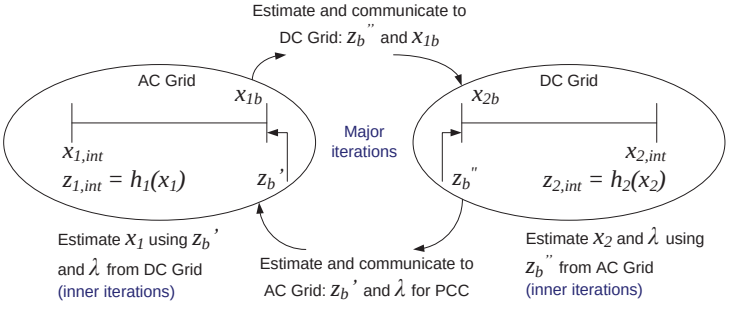

Figure 3: Data exchange across the boundaries during the iterations

VI. AC Grid Modeling

AC grid is modeled in a traditional manner [9]. Referring to Figure 3, power injection pseudo-measurements are assigned at the PCC buses and they are determined based on DC grid SE estimates from the previous major iteration. If the AC grid contains multiple sub-grids, they can be handled either sequentially or in parallel, given that they do not have any AC connections with each other.

VII. DC Grid Modeling

In this work, DC grid modeling focusses on VSC technology since this is the most relevant HVDC technology for larger HVDC Grids [1]. Three types of converter station configurations are considered, namely, bipole, asymmetric monopole and symmetric monopole. These are shown in Figure 4. It is assumed that all converters in a given DC grid have the same configuration. Different DC grids may have different configurations.

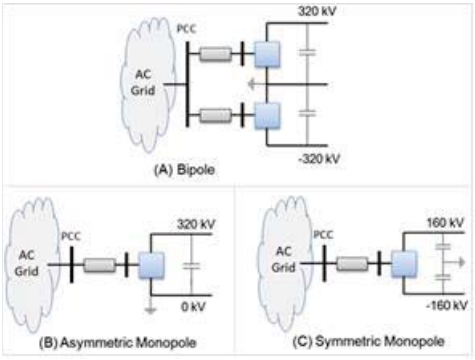

Figure 4: Configurations of VSC HVDC converter stations

Figure 5 shows the bipole configuration in more detail and various quantities related to the PCC bus, phase reactors, converter pole, DC buses and DC grid cables. These quantities can appear as measurements for the purpose of state estimation. The numbers in the parentheses enumerate the various measurement types considered in this work.

Monopole configuration is modeled as a subset of the bipole configuration. Only the measurements belonging to the positive pole of the bipole are considered while excluding other parts of the bipole model.

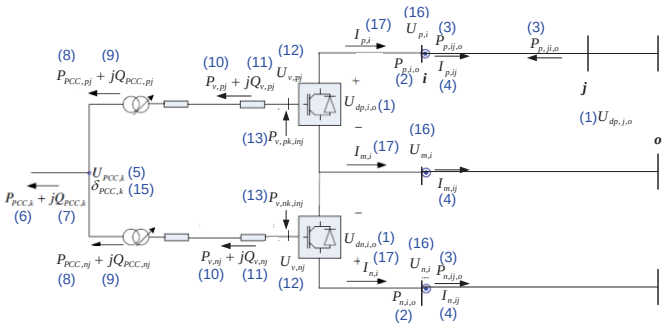

Figure 5: Bipole configuration and the measurement types

A. Modeling Parallel Converters in a Station

A converter station may have more than one converter that share a PCC bus, or a DC bus, or both. Figure 6 uses two monopole converters and DC grids as an example to facilitate the visualization of various configurations. Subscripts *p* and *m* refer to positive and metallic return networks. For the purpose of state estimation, if the parallel converters have separate PCC buses, each PCC bus needs to have its own voltage magnitude and angle states. Similar is applicable for the converter DC buses. Power flowing through the phase reactors of each parallel converter is treated as a separate flow measurement.

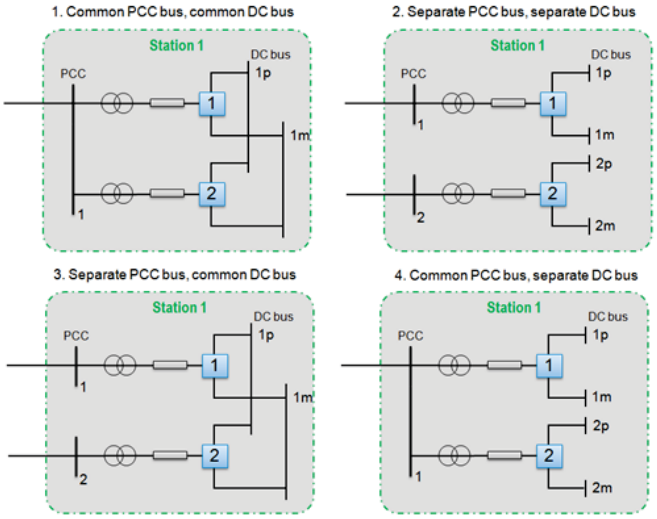

Figure 6: Configurations for two parallel monopole converters in a station

B. Modelling Converter-less DC buses

Some DC buses may not have a converter connected to it. This could be by design, or as a result of a circuit breaker operation and bus splitting. As an example, Figure 7 shows a DC grid with a monopole configuration. Bus 3 is a converter-less bus and there are two parallel converters in Station 1, sharing a DC bus.

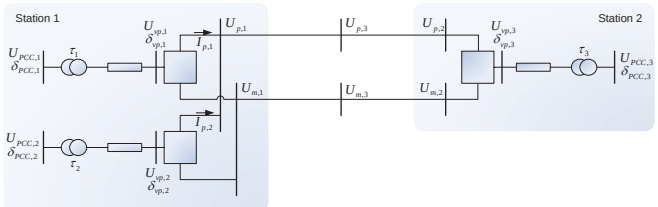

Figure 7: Two terminal monopole grid with a converter-less bus 3. Two parallel converters in Station 1 share a single DC bus

C. The State Vector

For a DC grid in a bipole configuration shown in Figure 5, the state vector x is defined for state estimation as:

$$\begin{bmatrix} U_{v,pj}\,,\delta_{v,pj}\,,U_{v,nj}\,,\delta_{v,nj}\,,\ldots,U_{PCC,k}\,,\delta_{PCC,k}\,,\ldots, \\ U_{p,i}\,,U_{m,i}\,,U_{n,i}\,,\ldots,\tau_j\,,\ldots \end{bmatrix}^T$$

Subscript j refers to a converter index, k refers to a PCC bus index and i refers to a DC bus index. In the state vector, the voltage magnitude and angle states $U_{v,pj}$, $\delta_{v,pj}$, $U_{v,nj}$, $\delta_{v,nj}$ for all converter pole buses are stacked together first, followed by the voltage magnitude and angle states $U_{PCC,k}$, $\delta_{PCC,k}$ for all the PCC buses in the DC grid, followed by the DC voltage states for all the DC buses $U_{p,i}$, $U_{m,i}$, $U_{n,i}$ in the DC grid, followed by the converter transformer tap position states τ_j for all converters.

Similarly, for a DC grid in a monopole configuration, the state vector x is defined as:

$$\begin{bmatrix} U_{v,pj}\,,\delta_{v,pj}\,,\dots,\ U_{PCC,k}\,,\delta_{PCC,k}\,,\dots, \\ U_{p,i}\,,U_{m,i}\,,\dots,\tau_j\,,\dots,I_{cp,j}\,,I_{cm,j}\,,\dots \end{bmatrix}^T$$

In the state vector, the voltage magnitude and angle states $U_{v,pj}$, $\delta_{v,pj}$ for all converter pole buses are stacked together first, followed by the voltage magnitude and angle states $U_{PCC,k}$, $\delta_{PCC,k}$ for all the PCC buses in the DC grid, followed by the DC voltage states for all the DC buses $U_{p,i}$, $U_{m,i}$ in the DC grid, followed by the converter transformer tap position states τ_j for all converters. To account for parallel converters in a monopole grid, the converter DC current states $I_{cp,j}$, $I_{cm,j}$ are have been added.

As an illustration, for the network in Figure 7, the state vector takes up the following form:

$$\begin{bmatrix} U_{v,p1}\,,\delta_{v,p1}\,,U_{v,p2}\,,\delta_{v,p2}\,,U_{v,p3}\,,\delta_{v,p3}\,,\dots, \\ U_{PCC,1}\,,\delta_{PCC,1}\,,U_{PCC,2}\,,\delta_{PCC,2},U_{PCC,3}\,,\delta_{PCC,3},\dots, \\ U_{p,1}\,,U_{m,1}\,,U_{p,2}\,,U_{m,2}\,,U_{p,3},U_{m,3},\dots, \\ \tau_1,\tau_2,\tau_3,\dots, \\ I_{cp,1}\,,I_{cp,2} \end{bmatrix}^T$$

D. The Measurement Function

Various types of DC grid measurements are considered as shown in Figure 5. They are also listed in Table 2 as a quick summary. Measurement functions are derived for each measurement type and the vector $h(x)$ is constructed by stacking up the individual entries for each measurement.

Table 2: The measurement types

Type	Measurement	Type	Measurement	Type	Measurement
(1)	$U_{dp,i,o}, U_{dn,i,o}$	(7)	$Q_{PCC,k}$	(13)	$P_{v,pj,inj}, P_{v,nj,inj}$
(2)	$P_{p,i,o}, P_{n,i,o}$	(8)	$P_{PCC,pj}, P_{PCC,nj}$	(14)	$I_{cp,bal}, I_{cn,bal}$
(3)	$P_{p,ij,o}, P_{n,ij,o}$	(9)	$Q_{PCC,pj}, Q_{PCC,nj}$	(15)	$\delta_{PCC,k}$
(4)	$I_{p,ij}, I_{m,ij}, I_{n,ij}$	(10)	$P_{v,pj}, P_{v,nj}$	(16)	$U_{p,i}, U_{m,i}, U_{n,i}$
(5)	$U_{PCC,k}$	(11)	$Q_{v,pj}, Q_{v,nj}$	(17)	$I_{p,i}, I_{m,i}, I_{n,i}$
(6)	$P_{PCC,k}$	(12)	$U_{v,pj}, U_{v,nj}$	(18)	$U_{bal,i}$

Measurement types (1)-(3) are DC bus voltage measurement, DC bus power injection measurement and DC cable power flow measurement respectively. These quantities are measured with respect to a midpoint bus o. Matrix G_p is a conductance matrix for the positive network of the DC grid. Type (4) is a DC cable current measurement. Type (5) is PCC bus voltage magnitude, types (6)-(7) are PCC bus active and reactive power injection measurements. For monopole converter station having parallel converters sharing a PCC bus, these measurement functions sum up the power flows over the phase reactors of the individual converters. Types (8)-(9) are the converter phase reactor active and reactor power flows measured at the PCC bus side, whereas types (10)-(11) are their counterparts on the pole valve bus side. Type (12) is the pole valve bus magnitude measurement. Type (13) is the pole valve bus zero power injection pseudo-measurement. For parallel monopole converters sharing a DC bus, type (14) pseudo-measurement is added that sums up the individual converter DC currents to the DC bus current injection. Measurement type (15) provides an angle reference to the AC parts of each converter station assembly. Type (16) is a DC bus voltage magnitude measured with respect to ground. Type (17) is a DC bus current injection measurement. Type (18) is a DC bus voltage magnitude pseudo-measurement for symmetric monopole to ensure that the positive and negative pole bus voltages are identical in magnitude.

A measurement Jacobian is required during the state estimation process. It is constructed by analytically differentiating the measurement function for each measurement type with respect to the state variables.

E. Contingency Modeling

Various contingencies such as out-of-service converter pole or DC cable are handled during the DC grid modeling. A bipole with an out-of-service converter pole is modeled using pseudo-measurements that set the appropriate pole reactor power flows and DC bus power injection to be zero. For instance, if a negative pole of bipole is out-of-service, pseudo-measurements as shown in Table 3 are introduced. In addition, the converter loss is set to zero.

Table 3: Pseudo-measurements for modeling negative pole out-of-service contingency

Measurement Type	Pseudo-measurements
(2)	$h(x) = P_{n,i,o} = 0$
(8)	$h(x) = P_{PCC,nj} = 0$
(9)	$h(x) = Q_{PCC,nj} = 0$
(10)	$h(x) = P_{v,nj} = 0$
(11)	$h(x) = Q_{v,nj} = 0$
(17)	$h(x) = I_{n,i} = 0$

A DC grid cable outage is modeled by appropriately modifying the DC grid conductance matrix for positive, negative and the mid-point network. For example, consider a simple DC grid with three DC buses connected to each other through DC cables. If cable connecting the buses 2 and 3 in the positive pole network is disconnected, the corresponding conductance matrix G_p will be given by

$$\begin{bmatrix} \frac{1}{R_{p12}}+\frac{1}{R_{p13}} & -\frac{1}{R_{p12}} & -\frac{1}{R_{p13}} \\ -\frac{1}{R_{p12}} & \frac{1}{R_{p12}} & 0 \\ -\frac{1}{R_{p13}} & 0 & \frac{1}{R_{p13}} \end{bmatrix}$$

The conductance matrices for the negative pole and mid-point networks remain unchanged.

When all the cables connecting a DC bus at a converter pole are out-of-service, the converter pole will not supply/absorb any power to/from the DC grid. Thus in such a scenario, the said converter pole is also modeled as being out-of-service. When all the cables in a particular (positive or negative) network containing bipole converters are out-of-service, the DC grid is modeled as a monopole converter network.

F. Other Features

The HVDC grid modeling also includes features such as grounding and wind farm connections. The following aspects have been considered in this work:

- The mid-point network of a DC grid may be grounded at a converter-station directly, through a resistance or may be left ungrounded. If no mid-point DC bus is grounded, voltage reference is provided by grounding any one converter arbitrarily. The grounding is reflected by modifying the DC grid conductance matrix of the mid-point return network appropriately.
- Wind farms are modeled either as a direct power injection measurement at PCC bus, or a power injection measurement at a collector bus connected to PCC bus through transmission cable, or they could be treated as any other AC grid during the major iterations of the distributed SE.

VIII. Examples and Testing

A hybrid AC/HVDC grid as shown in Figure 1 is used for illustration of the proposed distributed SE algorithm. The AC grid system consists of IEEE 39 bus network and IEEE 300 bus network. Figure 8 shows the hybrid grid network schematically. The DC grid system consists of two four-terminal bipole HVDC grids, one lying inside the 39 bus AC system and another connecting to the 300 bus AC system.

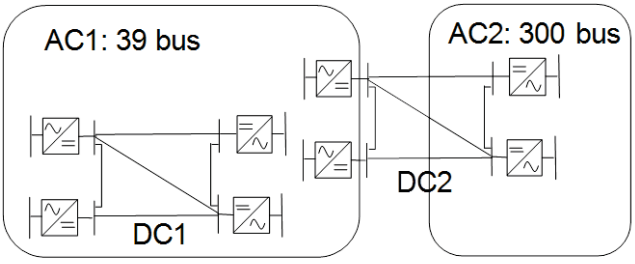

Figure 8: MAMD system with bipole HVDC grids

A. Convergence Criteria

Numeric behavior of the algorithm is analyzed using the two convergence criteria for terminating the iterative process:

- *Criterion A:* individual AC grid SE and DC grid SE are each executed until the inner iteration loop achieves converge before proceeding to the next major iteration.
- *Criterion B:* only a single inner iteration is carried out for AC grid SE and DC grid SE each. That is, the inner iterations are not necessarily run until convergence before proceeding to the next major iteration.

For both criteria, the major iterations are considered as converged once U_{PCC} mismatch between AC grid SE and DC grid SE estimates converges to within tolerance.

B. Test Case having Two Bipole HVDC Grids

The distributed SE algorithm based on network decomposition as proposed is run on the hybrid AC/HVDC system in Figure 8. Various AC and DC grid measurements are considered as described in the previous sections. Uniformly distributed measurement error between +/- three times standard deviation is added to simulate measurements.

Figure 9 shows the numerical behavior when Criterion A is used. Flat start is used for the 1st major iteration while the subsequent major iterations use warm start based on the previous iteration. Figure 9 (top) plot infinity norm of the difference between the PCC bus voltages estimated by AC grid SE and DC grid SE. Convergence is obtained at major iteration 5 and at convergence the mismatch is within tolerance 1e-4 p.u. That is, the PCC bus states estimated by AC and DC grid SE provide continuity at the boundaries of the decomposed networks. Figure 9 (bottom) plots the number of inner iterations for AC grid SE and DC grid SE for each major iteration. Due to the warm start of the major iterations, the inner iteration number for their respective convergence goes down as major iterations progress. In total, there are 5 major iterations and 27 inner iterations.

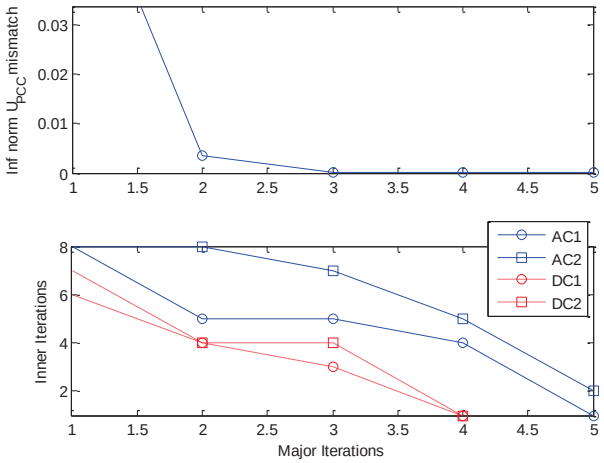

Figure 9: Criterion A: Infinity norm of U_{PCC} mismatch (top), inner iterations (bottom)

When Criterion B is used, only a single inner iteration of AC grid SE and DC grid SE is performed. Flat start is used for the 1st major iteration while the subsequent major iterations use warm start based on the previous iteration. This results in 13 major iterations and one inner iteration per major iteration until convergence. Figure 10 depicts the numerical behavior. In effect, Criterion B converges faster than Criterion A for the same specified tolerance.

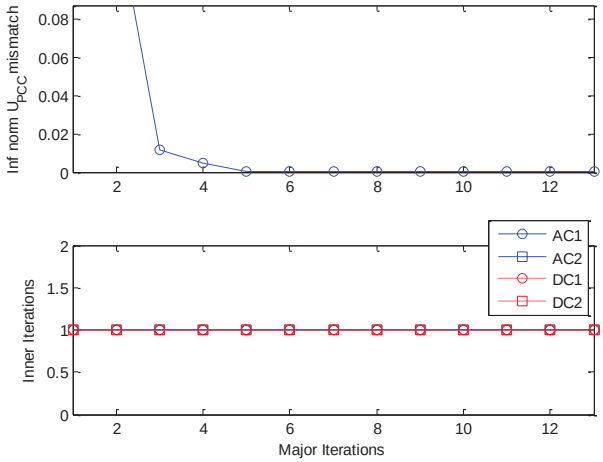

Figure 10: Criterion B: Infinity norm of U_{PCC} mismatch (top), inner iterations (bottom)

C. Test Case having Bipole and Monopole HVDC Grids

This test system is similar to the test case in Section VIII. B. except that DC Grid 1 has a symmetric monopole DC network. In addition, the DC grids have other features as summarized in Table 4.

Table 4: Features of test system

DC grids	DC1: symmetric monopole grid DC2: bipole grid
Parallel converters	DC1: converters 2 and 3 in parallel. Common PCC and DC bus.
Wind farm	DC1 PCC bus 2
Grounding	DC1: no grounding (symmetric monopole) DC2: solid grounding at DC bus 3, resistance grounding at DC bus 4.
Measurement noise	Uniformly distributed random noise: three times the standard deviation (max).

Convergence Criterion A is considered for this test case. Major iterations converge in four iterations. Table 5 summarizes the PCC bus power flows (from DC grid into AC grid), voltages and LaGrange multipliers at convergence. Note that the LaGrange multipliers for U_{PCC} are non-zero, that is, the PCC bus voltage equality constraint used in the combined SE formulation is binding and U_{PCC} is enforced to be equal within tolerance at convergence. On the other hand, LaGrange multipliers for δ_{PCC} are insignificant, consistent with the fact that an angle reference for the AC part of each converter station can be set independently of other stations and other grids.

Table 5: PCC bus estimates at convergence

PCC	P_{PCC} (MW)	Q_{PCC} (MVAR)	U_{PCC} (pu)	δ_{PCC} (deg)	λ_{UPCC}	$\lambda_{\delta PCC}$
1	585.75	16.29	1.01	7.48	93.64	7.28e-12
2	-592.94	39.01	1.00	0.00	-123.09	4.26e-14
3	-574.48	-1.60	1.00	-3.24	11.82	1.51e-10
4	523.82	101.00	1.03	24.79	-77.60	-1.22e-10
5	800.09	1.46	1.03	2.80	77.50	-7.98e-10
6	-801.15	189.08	1.01	-10.80	233.80	-8.53e-10
7	-800.92	-7.02	0.94	-11.61	104.28	1.22e-09
8	761.00	1.71	1.06	11.46	11.17	2.37e-10

Figure 11 shows a plot of DC grid measurement residuals scaled by the standard deviations of the measurements to provide approximate values of the normalized residuals. As apparent from the figure, they are less than 3, which agree with that the measurement error introduced was at most 3 times the standard deviation.

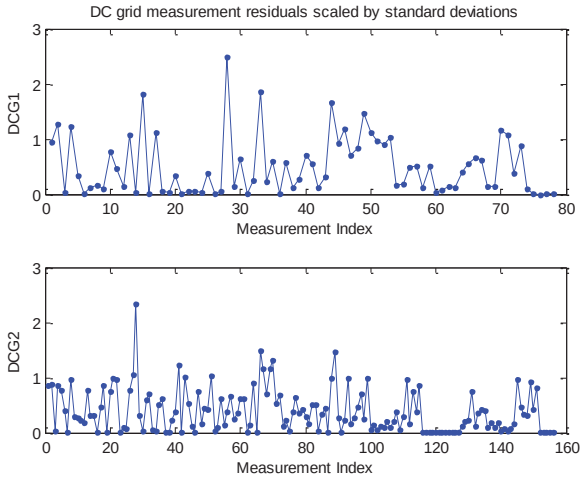

Figure 11: DC grid measurement residuals

D. Test Case having Bipole and Monopole HVDC Grids and Various Modeling Features

This test case uses the same nominal network as in Section VIII. C. and few additional features are introduced to emphasize the modeling capability of the method. Figure 12 (left) shows the network schematically. In DC Grid 1, there are converter-less buses and a DC cable out-of-service. In DC Grid 2, negative pole of a converter and a DC cable in the positive DC network are out-of-service. The distributed AC/HVDC SE algorithm converges in three major iterations using Criterion A. The major iterations are summarized in Figure 12 (right).

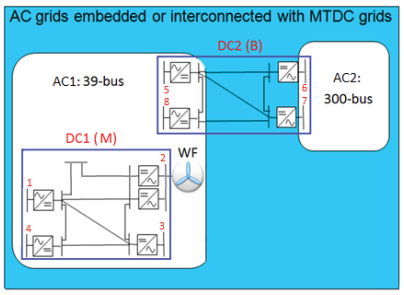

Major Iter	U_{PCC} estimate mismatch (p.u.)
1	9.1e-2
2	1.4e-4
3	9.5e-5

Figure 12: (left) the test system with monopole (M) and bipole (B) grids, (right) major iterations and PCC state mismatch

IX. Conclusions

A distributed algorithm for state estimation is designed that is appropriate for hybrid AC/HVDC grids. It is based on network decomposition which is naturally provided by the hybrid AC/HVDC grids. Techniques building upon LaGrangian relaxation and blockwise Gauss-Seidel approach are used to solve the resulting system of nonlinear equations. Coordinator program houses the proposed algorithm and coordinates the data exchanges between major iterations. Only

the PCC data needs to be exchanged thus resulting in minimal data communication requirements during runtime. The method supports multiple AC and VSC HVDC grids, monopole and bipole configurations, parallel converters, converter-less DC buses, contingency situations, various types of grounding and converter tap position estimation. The algorithm has been successfully tested and validated with a relevant IEEE 39 and 300 bus AC grids along with monopole and bipole HVDC grids.

X. References

[1] CIGRE Technical Brochure 533 2013, B4-52 HVDC Grid Feasibility Study

[2] M. Callavik, M. Bahrman, and P. Sandeberg, "Technology Developments and Plans to Solve Operational Challenges Facilitating the HVDC Offshore Grid", IEEE PES General Meeting 2012

[3] J. Carvalho, F. Barbosa, "Distributed Processing in Power System State Estimation", Mediterranean Electrotech Conf, MEleCon 2000, Vol. III

[4] R. Ebrihimian, R. Baldick, State Estimation Distributed Processing, IEEE Transactions on Power Systems, Vol. 15, No. 4, Nov 2000

[5] T. Yang, H. Sun, A. Bose, Transition to a Two-Level Linear State Estimator—Part II Algorithm, IEEE Transactions on Power Systems, Vol. 26, No. 1, Feb 2011

[6] A. Jaén, E. Acha, A. Expósito, "Voltage Source Converter Modeling for Power System State Estimation: STATCOM and VSC-HVDC," IEEE Transactions on Power Systems, Vol. 23, No. 4, Nov 2008

[7] Q. Ding, T. Chung, B. Zhang, "An Improved Sequential Method for AC/MTDC Power System State Estimation," IEEE Transactions on Power Systems, Vol. 16, No. 3, Aug 2001

[8] S. Hongbin, L. Dazhi, Z. Boming, L. Chongru, "Method for the status estimation of the AC/DC mixed power system," Chinese Patent Application # 200710065198

[9] A. Monticelli, State Estimation in Electric Power Systems A Generalized Approach, Kluwer publishers 1999

XI. Biographies